SAW-driven electron dynamics in nanostructures

The acoustoelectric effect is the manifestation of the transport of charge carriers in a piezoelectric semiconductor by means of surface acoustic waves (SAWs). Lattice deformations induced by SAWs in a piezoelectric substrate generate potential waves that can drag electrons resulting in a net dc current or voltage [1] also in an intrinsic medium if electrons are fed into the device by an appropriate injector [2].

In one-dimensional (1D) devices, this effect gives rise to acoustoelectric current quantization [3]: control over the 1D-constriction width allows the accurate determination of the number of electrons packed in each SAW-potential minimum down to single-electron transport.

The demonstration of quantized acoustoelectric effect led to the proposal of several innovative devices: converting the flux of individual SAW-driven electrons in a flux of photons by injecting them into a two-dimensional hole gas, would realise an almost ideal single-photon source for quantum-cryptography applications. Additionally, manipulation of single electrons in 1D systems can be exploited to implement scalable quantum-information-processing circuits with solid-state devices. At NEST we are exploring these approaches aiming at the realisation of a high-repetition-rate single-photon source [4] and a solid-state Hadamard gate based on a three-terminal Aharonov-Bohm ring which is investigated in the linear-transport regime.

Vincenzo Piazza

v.piazza@sns.it

Collaborators
F. Beltram
G. Biasiol
G. De Simoni
L. Sorba
E. Strambini

SAW-driven single-photon source

Our scheme (Fig. 1a) is based on a *n-i-p* planar junction defined in a quantum well in a GaAs/AlGaAs heterostructure: SAWs, propagating from the *n*-side of the device to the *p*-side drive electrons along the *i*-region towards the *p*-region where radiative recombination occurs. A 1D constriction will allow controlling the acoustoelectric current down to the single electron regime. In this condition at most one photon per SAW cycle is generated.

A *n*-region and a *p*-region are induced by *n*-type and *p*-type Ohmic contacts and two top gates that allow inducing in the QW a two-dimensional electron gas (2DEG) and a two-dimensional hole gas (2DHG). The central sections of the gates (Fig. 1a) incorporate narrow structures (NSs) to select a privileged area for *n-i-p* conduction that can be electrostatically controlled by a pair of lateral gates (LGs). An interdigitated transducer (IDT), with a resonance frequency of 3.018 GHz, generates SAWs that propagates from the *n* to the *p* side of the device.

Acoustoelectric transport was probed at 5 K by injecting a constant current into one of the *n*-type contact (the *n*-source) while measuring the current flowing out from another contact (the *n*-drain). A 2DHG was also induced in the *p*-region and a current injected between the *p*-source and the *p*-drain.

At the IDT resonance, carrier transfer between the two regions is observed as a negative peak in the *n*-drain current (Fig. 2a). The electrons transferred into the 2DHG region recombine with holes resulting in a positive peak in the *p*-drain current and in an electroluminescence (EL) signal due to electron-hole radiative recombination. Spatially-resolved snapshots of EL emission

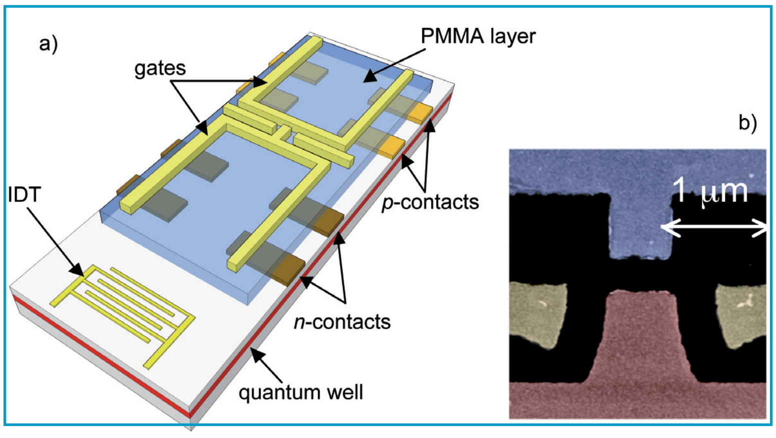

Fig. 1
a) Schematic view of the SAW-based single photon source. SAWs, generated by the interdigital trasnducer (IDT), extract electrons from the n-type region and drag them to the p region where radiative recombination occurs. The 1D constriction in the central part of the device allows controlling the current.
b) coloured SEM image of the SAW-based device. The red (blue) region is the gate that controls the n-type (p-type) side of the junction. Yellow areas are the lateral gates that allow tuning the 1D constriction width.

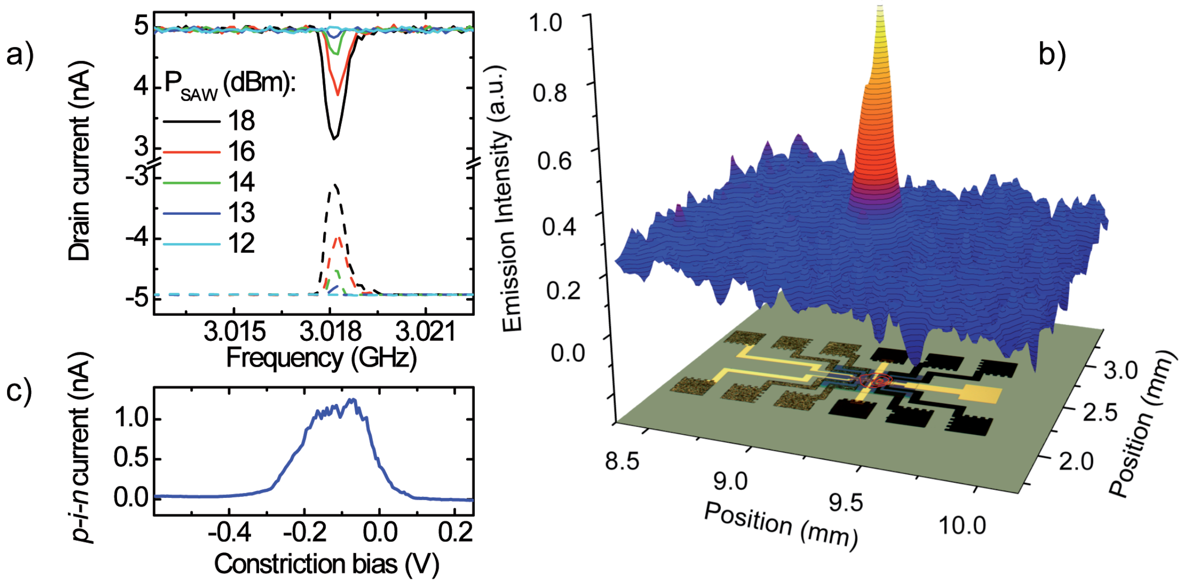

Fig 2.
a) *n*-drain (solid) and *p*-drain (dashed) current as a function of the IDT excitation frequency at different excitation power levels when a fixed current of -5 nA (5 nA) was injected into the *n* (*p*) source. Out of resonance the carriers injected from the sources reach the drains of the same type. At resonance electron transport from the *n* to the *p* part is observed. **b)** Emission intensity in presence of SAW with a frequency of 3.018 GHz and 15 dBm of power as a function of position superimposed on an optical image of the device. The EL signal is centred on the NSs. **c)** *n-i-p* SAW driven transport as a function of the bias applied to the LGs. The IDT was excited at resonance (3.018 GHz) at a power of 18 dBm. Complete pinch-off of the current was observed both for positive and negative bias values.

confirm that emission occurs from the NSs (Fig. 2b). Figure 2c shows that the constriction can be narrowed down to complete acoustoelectric-current pinch-off by means of the LGs.

Device optimization is currently being carried out to demonstrate single-photon operation.

SAW-driven flying qubits

SAW-driven single-electron wave packets can be used as *flying qubits* in 1D channels [5]. Within this scheme the qubit consists of two adjacent 1D channels, called the 0- and the 1-rail, respectively. The logical state |0⟩ (|1⟩) is determined by the presence of the SAW-driven single electron in the 0-rail (1-rail) [6]. Our approach exploits the Aharonov-Bohm (AB) effect to allow control on the phase of the electronic wavefunction at the outputs. Multiterminal Aharonov-Bohm rings were theoretically analyzed by means of scattering-matrix approaches in the Landauer-Büttiker framework, free electron-like node equations, and displaced Gaussian wavefunctions [7,8]. At NEST we extended existing theories based on scattering-matrix approaches by including the effect of decoherence and classical (Lorentz) forces in the description of the system and carried out a comparison against experimental results on real devices by studying the low-temperature coherent-transport properties of three-terminal AB rings. Our analysis shows that the inclusion of these effects is necessary to fully understand the observed phenomenology.

Three-terminal AB rings were fabricated from a two-dimensional electron gas (2DEG) confined in a GaAs/AlGaAs heterostructure (Fig. 3a).

The second derivative of $g_t = g_2 + g_3$ with respect to B, where $g_i = I_i/V_{ex}$, I_i the output current from lead i, and V_{ex} the excitation signal applied to L_1, is reported in Fig. 4a as a function of B and V_{G2}, measured at a temperature of 350 mK.

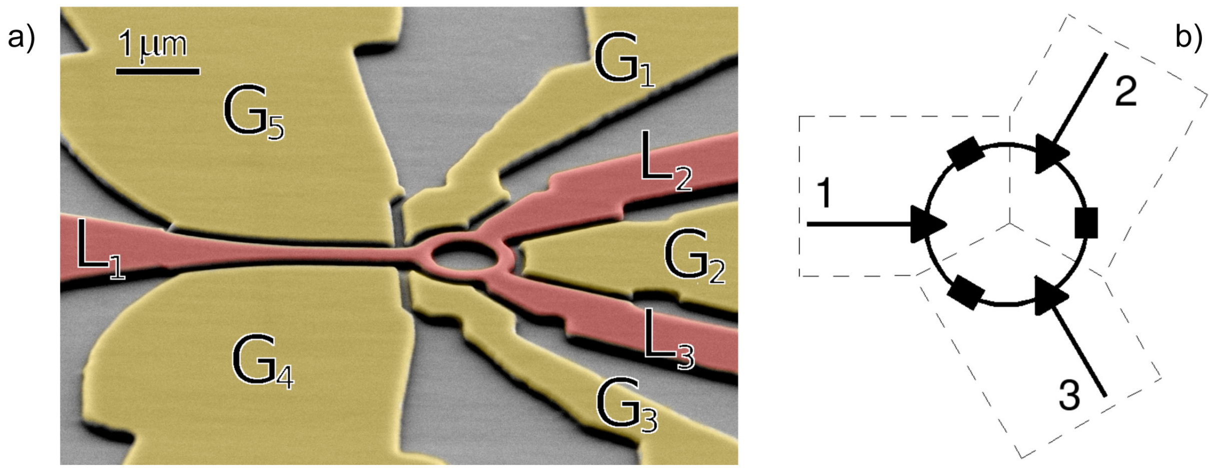

Fig 3
a) SEM image in artificial colours of one of our three-terminal rings (red area). The brown portions of the 2DEG are used as lateral gates to control the conductivity and phase of the ring. **b)** Scheme of a three-terminal ring used in our model.

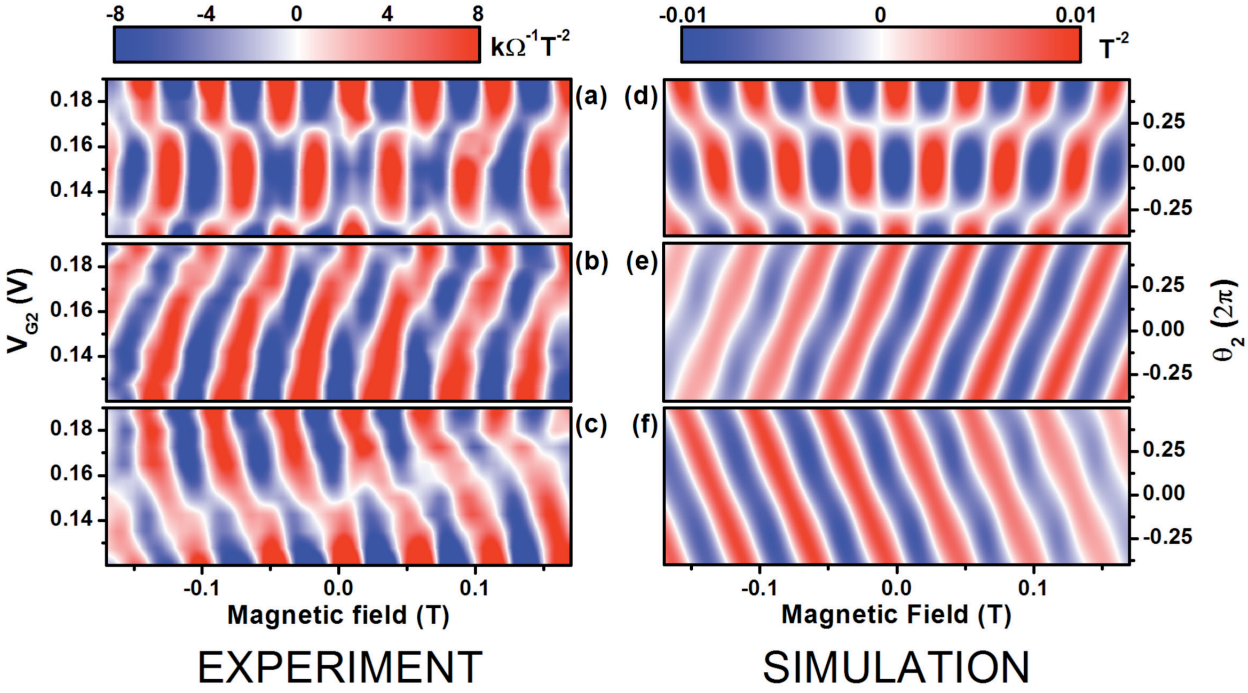

Fig 4
Contour plots of the second-order derivatives of g_2+g_3 (panel a), g2 (panel b), and g3 (panel c) with respect to the magnetic field as a function of B and V_{G2} and comparison with the results obtained by best-fitting the data with our model (panels d, e, and f)

It is symmetric with respect to B in the entire range of gate voltages explored. In the region between -0.1 T and 0.1 T abrupt jumps of the oscillation phase from 0 to π can be seen at V_{G2} = 0.17 V and V_{G2} = 0.125 V, reminiscent of the phase-rigidity phenomena observed in two-lead, closed rings [8]. At larger magnetic fields, these phase jumps become smoother, and evolve towards an almost continuous shift of the phase with gate bias. A remarkably different behaviour was observed in the evolution of the individual outputs as a function of B and V_{G2}, shown in Fig. 4b and 4c. In this case, the phase of the oscillations of g_2 evolves almost linearly with V_{G2} in the entire range of magnetic fields and gate voltages explored. g_3 shows a similar behaviour, but with an opposite dependence of the phase evolution on V_{G2}.

We schematised our three-terminal rings with the three identical blocks shown in Fig. 3b, where triangles represent three-terminal scatterers and rectangles include the evolution of the wavefunction phase [9]. The effect of the Lorentz force is included by introducing an asymmetry in the branching probability of each scatterer. Decoherence effects are modelled with absorbers located in the arms: with this approach our model is able to describe the evolution of the coherent part of the wavefunction.

A comparison between simulated and experimental total output of our ring is plotted in Fig. 4. Inspection of this Figure confirms the ability of our model to provide an accurate description of the experimental data.

References

[1] A. Esslinger, A. Wixforth, R.W. Winkler, J. P. Kotthaus, H. Nickel, W. Schlapp, and R. Lsch, Solid State Commun. 84, 939 (1992).
[2] M. Cecchini, G. de Simoni, V. Piazza, F. Beltram, H. E. Beere and D. A. Ritchie, Appl. Phys. Lett. 88, 212101 (2006).
[3] J. M. Shilton, V. I. Talyanskii, M. Pepper, D. A. Ritchie, J. E. F. Frost, C. J. B. Ford, C. G. Smith and G. A. C. Jones, J. Phys.: Condens. Matter 8, L531 (1996); J. Cunningham, V. I. Talyanskii, J. M. Shilton, M. Pepper, A. Kristensen and P. E. Lindelof, Phys. Rev. B 62, 1564 (2000).
[4] Giorgio De Simoni, Vincenzo Piazza, Lucia Sorba, Giorgio Biasiol, and Fabio Beltram, Appl. Phys. Lett. 94, 121103 (2009).
[5] A. Bertoni, P. Bordone, R. Brunetti, C. Jacoboni, and S. Reggiani, Phys. Rev. Lett. 84, 5912 (2000); C. H. W. Barnes, J. M. Shilton, and A. M. Robinson, Phys. Rev. B 62, 8410 (2000).
[6] R. Ionicioiu, G. Amaratunga, F. Udrea, Int.J.Mod.Phys. B 15, 125 (2001).
[7] C. H. Wu and D. Ramamurthy, Phys. Rev. B 65, 075313 (2002); 2 D. Ramamurthy, and C. H. Wu, Phys. Rev. B 66, 115307 (2002); S. Datta, M. Cahay, and M. McLennan, Phys. Rev. B 36, 5655 (1987); M. Cahay, M. McLennan, and S. Datta, Phys. Rev. B 37, 10125 (1988); C. H. Wu, and G. Mahler, Phys. Rev. B 43, 5012 (1991); B. Szafran and F. M. Peeters, Europhys. Lett. 70, 810 (2005).
[8] A. Yacoby, R. Schuster, and M. Heiblum, Phys. Rev. B 53, 9583 (1996); A. Aharony, O. Entin-Wohlman, T. Otsuka, S. Katsumoto, H. Aikawa, and K. Kobayashi, Phys. Rev. B 73, 195329 (2006).
[9] E. Strambini, V. Piazza, G. Biasiol, L. Sorba, and F. Beltram, Phys. Rev. B 79, 195443 (2009).